Robotica (2016) volume 34, pp. 2163–2185. © Cambridge University Press 2014
doi:10.1017/S0263574714002811

Robotic hand posture and compliant grasping control using operational space and integral sliding mode control

Guido Herrmann*†, Jamaludin Jalani‡, Muhammad Nasiruddin Mahyuddin§, Said G Khan¶ and Chris Melhuish‖

†*Bristol Robotics Laboratory, Department of Mechanical Engineering, Faculty of Engineering, University of Bristol, BS8 1TR, United Kingdom. E-mails: mexgh@bris.ac.uk*
‡*Department of Electrical Engineering Technology, Faculty of Engineering Technology, Universiti Tun Hussein Onn Malaysia, 86400, Parit Raja, Batu Pahat, Johor, Malaysia*
§*School of Electrical and Electronics Engineering, Universiti Sains Malaysia, Pulau Pinang, Malaysia*
¶*Department of Mechanical Engineering, College of Engineering Yanbu, Taibah University, Saudi Arabia*
‖*Bristol Robotics Laboratory, University of the West of England, Bristol, BS34 8QZ, United Kingdom*

(Accepted 21 November 2014. First published online: December 23, 2014)

SUMMARY
This paper establishes a novel approach of robotic hand posture and grasping control. For this purpose, the control uses the operational space approach. This permits the consideration of the shape of the object to be grasped. Thus, the control is split into a task control and a particular optimizing posture control. The task controller employs Cylindrical and Spherical coordinate systems due to their simplicity and geometric suitability. This is achieved by using an integral sliding mode controller (ISMC) as task controller. The ISMC allows us to introduce a model reference approach where a virtual mass-spring-damper system can be used to design a compliant trajectory tracking controller. The optimizing posture controller together with the task controller creates a simple approach to obtain pre-grasping/object approach hand postures. The experimental results show that target trajectories can be easily followed by the task control despite the presence of friction and stiction. When the object is grasped, the compliant control will automatically adjust to a specific compliance level due to an augmented compliance parameter adjustment algorithm. Once a specific compliance model has been achieved, the fixed compliance controller can be tested for a specific object grasp scenario. The experimental results prove that the Bristol Elumotion robot hand (BERUL) can automatically and successfully attain different compliance levels for a particular object via the ISMC.

KEYWORDS: Robotic hand; Grasping posture; Compliant control; Power grasping; Integral sliding mode control.

1. Introduction

Emulating the human hand via a robot hand to perform a grasping task can be challenging.[1–4] Providing sufficient knowledge of the object geometry is an important criterion in order to plan motions and compute successful grasps.[5–9] Interesting results from Akin *et al.*[6] can assist researchers to plan their grasping technique. These results show that over 50% of the required grasps are cylindrical, and it is possible for a three-fingered hand to achieve over 90% of these grasps using a cylindrical design

* Corresponding author. E-mail: g.herrmann@bris.ac.uk

approach for the hand mechanics. Similar results which suggest a cylindrical geometry method can also be found in ref. [7]. This lead Akin *et al.*[6] to the design of a robotic hand, while Geng *et al.*[7] derived an approach to transfer human grasping postures to the kinematic positioning of a three fingered hand, using also neural network learning techniques to achieve matching. Thus, for a suitable grasping geometry, a tested cylindrical coordinate system as in refs. [6] and [7] can be very helpful. In contrast, the work in refs. [5], [8] and [9] promotes a spherical reference system for the objects which are to be grasped. Similar to ref. [7] this leads to an analysis of robotic two and three fingered hands for suitable robotic hand postures/positioning, which can be incorporated into robotic hand manipulation processes such as grasping or pinching. The analysis of Gioioso *et al.*[9] advances over that as it also considers the precise analysis of forces in the human-robot hand mapping strategies. This lead for Gioioso *et al.*[9] to a detailed simulation analysis of an object model map.

When touching an object, a (power) human hand does not require very high accuracy for the finger positioning and orientation. The grasping task needs to guarantee that the fingers sufficiently surround the object, staying in good contact and creating a suitable ergonomics-inspired posture.[10] As a result of such analysis, the authors of this paper suggested for hand positioning for grasp and for grasping an object-based coordinate system (see early ideas in refs. [11] and [12]); hence, this choice of coordinate system focuses on the object shape. Thus, the control is carried out in relation to the object shape rather than in a global Cartesian coordinate frame. This allows for radial thumb abduction in a pre-grasp positioning exercise of the fingers (all other fingers of our hand follow a cylindrical coordinate system), while finger-object forces are practically controlled using an active compliance control approach, in contrast to a detailed analysis, e.g., ref. [9]

The hand pre-grasping and actual grasping control may be split into a *task* where the fingertips move towards the object, while the fingers overall retain a suitable *posture* to permit good contact in a grasping exercise. A simple way to achieve this desired grasping is by using the operational space approach.[13] The underlying concept of the operational space approach is based on the decomposition of the control signal into *task* and *posture* control. This geometric splitting may have some similarity to the hybrid force/velocity approach in ref. [14] (pp. 396). However, the operational space control approach lends itself to a control approach where a high accuracy finger joint trajectory can be avoided. Exploiting the task controller allows the fingertip to reach a target position of the object through spherical coordinates for the thumb and cylindrical coordinates for the other fingers while the ergonomics-inspired, posture controller keeps a nominal finger posture as much as possible and does not need high accuracy. This allows good enclosure of the object by the controlled fingers. This idea together using in particular the ISMC as task compliance controller is elaborated on here in this paper in detail.

Thus, this paper will also provide suggestions to one of the functions required by a robot hand when used in fragile object manipulation or human-robot interaction: the ability to grasp any objects without damage. For this, a compliant control strategy is important to provide such grasping technique.[15] Some effort has been devoted to realize compliant passive grasping.[16–19] Hence, this work was mainly based on passive mechanical compliance which is not easily tunable once practically implemented. In particular for (anthropomorphic) hands and grippers,[20,21] the introduction of a mixed compliance system in the joints, actuators, and also fingertips can be highly beneficial to the grasping process, but certainly a challenge to manipulation.

Different active compliant control strategies have been proposed by refs. [22]–[26]. Hybrid force-position control is widely used to handle gripping or grasping of objects;[27] the control approach introduces two states.[28,29] The first state is controlling the positioning error which is also known as controlling an unconstrained mode while the second state is providing force control in a particular direction. Between these two states, there is a transition mode from positioning control to force control. Early controllers resolved this through a switching mode[29] which may be discontinuously achieved. Switching actions may be uncertain and cause instability.[30] More recent solutions have resolved this in a geometric approach, where the directionality expressed by the kinematics Jacobian defines the directions for position and force control.[14,27,30] Directional force control approaches are ideal in industrial applications,[29] but may be generally problematic in scenarios with humanoid robot hands, where the environment is uncertain and multidirectional (although specific exceptions of directional compliance control in robot hands exist[27]).

In contrast, compliance control has been achieved due to the definition of virtual spring-damper systems.[23–26,31] For instance, force/torque sensors have been used to close local force/torque loops

https://doi.org/10.1017/S0263574714002811 Published online by Cambridge University Press

to overcome joint flexibilities and uncertainties.[23,24,26,32] These schemes introduce the ability of directly tunable spring-damper interaction via a two loop structure: an internal loop controls a torque tracking structure, while an actively controlled spring-damper system is created in an outer loop. This can be improved by observer-based techniques[33,34] to differentiate external and intrinsic forces and torques (e.g., friction). Nevertheless, accurate model information of the robotic manipulator is required to tune the spring-damper system as shown in refs. [23], [24], [26] and [32]. However, a practical robot model is usually not easily identified and uncertain, rendering also the tuned spring-damper system as uncertain. In this respect, a solution to the compliant control problem in grasping has been presented by ref. [35] using a combination of an adaptive contact force observer, an environment parameter estimator, an adaptive sliding-mode friction compensator, while Zhang *et al.*[35] foresee a strong improvement of their results by the future inclusion of an advanced tactile sensor system.[36,37] Considering the comments above, the introduction of robustness to model and environmental uncertainty into compliance control is essential.

In this paper, ISMC using a model reference idea will be discussed. The reference model will introduce an exact virtual mass-spring-damper system which will determine the compliant control characteristics, i.e., the ISMC approach is not switching between two different states. ISMC (see refs. [38] and [39] for tracking) is a control approach which can counteract system uncertainties and is particularly useful for mechanical systems with stiction and friction and small negligible flexibilities as the robot hand. For such systems, ISMC is an almost model free control approach, i.e., it permits large system uncertainties and does not require accurate model knowledge as needed for feedback linearization/dynamic inversion schemes; sliding mode control can overcome these requirements with a high gain control element. Thus, ISMC is robust to model uncertainties and the reference model idea avoids the switching between different states as in hybrid control. Hence, the ISMC controller permits for motion planning and for compliance control due to the inherent model reference characteristics built into ISMC. For compliance, it is desirable that the robot hand is able to adapt to different compliance levels. Humans can effortlessly grasp and manipulate their hand compliance levels for specific objects. This can be realized through the automatic alteration of the reference model in an *initial* tuning process, in particular when a (measured) force signal is exerted on an object.

In contrast to former, seemingly more complex work, this work offers a simplified (power) grasping approach which permits collision-free pre-grasping and grasping with well-defined forces using the novel synergetic integration of the following active control techniques:

- Control of a robot hand via the operational space approach using spherical and cylindrical coordinates for pre-grasping positioning and grasping control.
- Robust finger (i.e., hand) posture optimization via a robust sliding mode posture controller (recently suggested for a torso robot[40]) which allows for a practical, simple and ergonomically relevant grasping trajectory and which reduces the need for high accuracy.
- Introduction of a novel compliance reference model controller, where the reference model is subject to an external measurement signal and is to be used in the novel context of the ISMC (this avoids scheduling methods, hybrid compliant control approaches and exact robot hand model information).
- Robust compliant control which is non-switching between operating modes, including theoretical guarantees.
- Suggestion of an automatic tuning procedure for the compliance reference model for practical force-object interaction.

Most importantly the results are *practically demonstrated.* Hence, we also extend significantly over our own recent work on compliant grasping (refs. [11] and [12]), by providing a comprehensive theoretically and practically founded discussion for the complete, combined framework of our robotic hand grasping technique.

2. The Elumotion Hand and Its Use within a Cylindrical and Spherical Coordinate System

Figure 1 shows the BERUL hand. It is to note that all fingers, i.e., index, middle, ring, and small finger consist of three links and three joints except the thumb finger. The thumb has four joints and four links. For the majority of the fingers, these joints are connected through a single, flexible pushrod which is then actuated by a leadscrew mechanism that converts a rotary movement of the electrical

https://doi.org/10.1017/S0263574714002811 Published online by Cambridge University Press

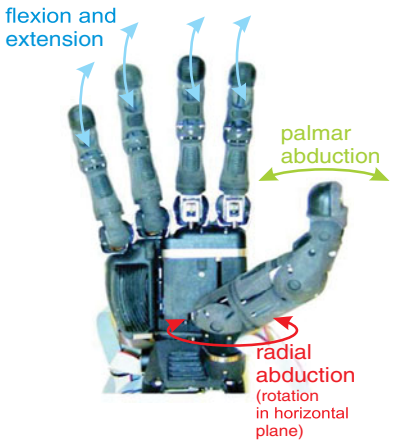

Fig. 1. An underactuated BERUL hand with available finger motion.

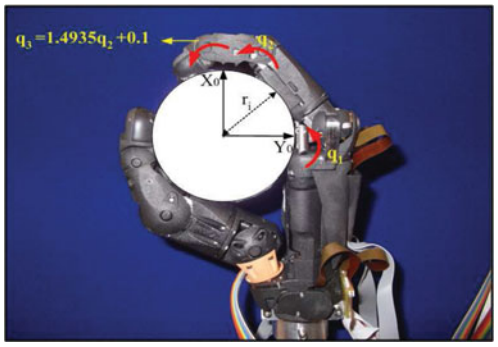

Fig. 2. Cylindrical coordinate system used for index, middle, ring and small fingers (joint positions in [rad]).

motor into a linear movement. Nine servo motors have been attached to various fingers of the BERUL hand. In particular, one motor actuator is used for the small and ring finger and two actuators used for the middle, index and thumb finger. Although the *middle and index fingers* are having two actuators, they follow a planar motion (flexion/extension, see Fig. 1).

In contrast, the thumb end-effector motion is more complex due to the two applied actuators and their mechanisms: one actuator is used for the push-rod mechanism (i.e., for palmar abduction), while the other motor introduces rotational motion similar to radial abduction in a human thumb (see Fig. 1).

Since all the fingers are constrained due to the use of the push-rod and leadscrew mechanism, the actuation of the first link (proximal phalange) of each finger will create a relational movement of the other links (intermediate and distal phalanges). Measurement of the kinematics of each finger showed that the relationship of the joint movement is sufficiently linear, so that the effect of the pushrod constraining the fingers can be modelled similar to a pulley belt system and the discussion can be found in ref. [41] (see Figs. 2 and 3). This allows a reasonably accurate computation of the end positions of each fingertip via forward kinematics in the targeted spherical/cylindrical coordinate system using the motor position, i.e., the first directly actuated joint angle values of each finger, and the linear relationship between each joint angle.

In general, the BERUL hand is able to closely mimic real hand movements and approximate humanlike speeds. For this paper, we focus on the ring, index and thumb finger, as examples of fingers with one and two actuators with planar and non-planar motion.

In order to allow for practical grasping for the BERUL fingers, we exploit the cylindrical and the spherical coordinate system. The cylindrical or the spherical coordinate system can be centred at the object to be grasped (see Figs. 2 and 3 for the coordinate system placement). Note that the transformation between joint, Cartesian and cylindrical/spherical coordinates follows a standard mathematical calculation. The cylindrical coordinate system is most suited to the index, middle, ring

https://doi.org/10.1017/S0263574714002811 Published online by Cambridge University Press

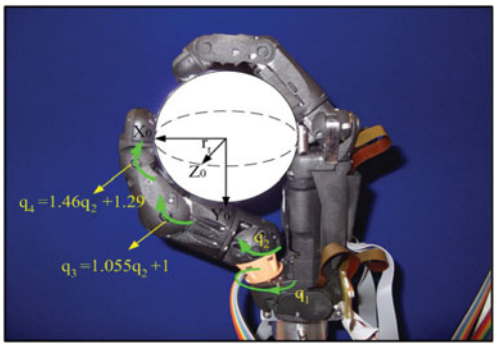

Fig. 3. Spherical coordinate system used for thumb finger (joint positions in [rad]).

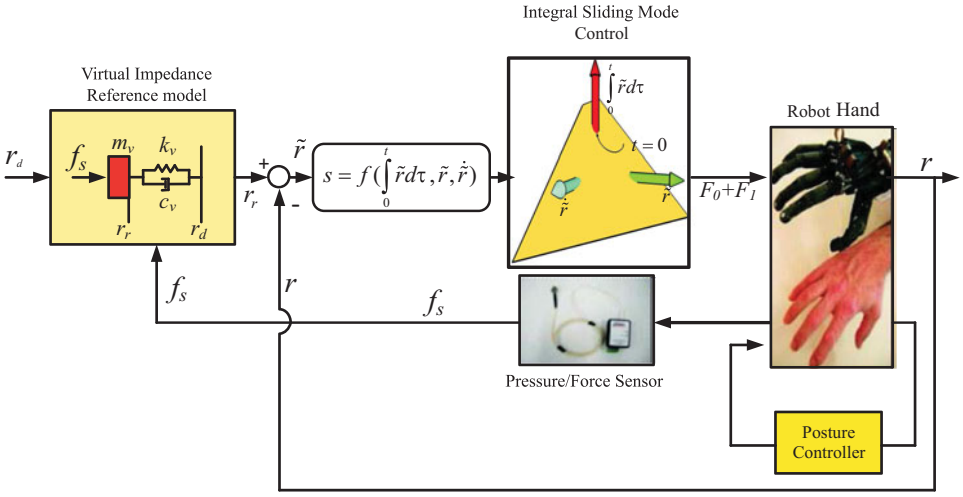

Fig. 4. Block diagram of the ISMC to achieve active compliance control for the BERUL fingers.

and small fingers, since these fingers often follow a planar movement, even when they are having several actuators. A thumb generally is more versatile in its movements, as it has to move from its initial position around objects (palmar and radial abduction). Thus, spherical coordinates are suited for the thumb. For grasping, it is not necessary to control the joint position of each finger at a high accuracy. Grasping can be easily directed by the radial position r of the fingertip and a preferred posture in case fingers are multi-redundant. Hence, both the cylindrical and spherical coordinates lend themselves to finger control via the radius r.

3. Controller Structure

The overall structure for the active compliance controller of the BERUL fingers is depicted in Fig. 4. We employ the operational space approach, which allows the geometric splitting into task and posture control, creating two parts in the control scheme. The first part is the ISMC based compliance controller for the task, controlling the radial coordinate of each finger in the cylindrical or spherical coordinate system. The task controller introduces a virtual reference model for compliant (power) grasping in the virtual coordinate r_r, representing a mass-spring-damper system considering a virtual mass m_v, spring with coefficient k_v and damping with coefficient c_v subjected to an external force, f_s. This force is sensed through a pressure sensor, creating motion r_r relative to the desired reference position r_d. Thus, providing a virtual impedance/compliance model for the finger motion under the effect of external forces. The robust ISMC enforces that the radial position r of the finger follows r_r at any time (to be explained in Sections 3.1.1 and 4). The second part of the controller, the posture controller introduces suitable motion of redundant degrees of freedom in particular for the thumb or index finger.

https://doi.org/10.1017/S0263574714002811 Published online by Cambridge University Press

A general model of a robot is

$$M(q)\ddot{q} + V(q, \dot{q})\dot{q} + G(q) + D_f = \tau. \tag{1}$$

where M, V and G provide mass, velocity and gravity terms, respectively. The vector D_f represents amplitude limited friction and stiction disturbances and uncertainties; in addition, D_f can also represent forces which result from interaction of the hand with other objects.[(1)] The torque vector τ represents the external actuating torques affecting each joint. This representation certainly holds for each specific finger for which we develop here the controller, in particular also for the push-rod actuated fingers.[39] It is to point out that in the context of the robot hand, the term $V(q, \dot{q})\dot{q}$ has very little significance. However, the terms $G(q)$ and D_f clearly have significant influence, considering that the practical BERUL hand is to be attached and moved with the robot arm. Moreover, friction and stiction has significant effect due to the push-rod mechanism.

3.1. Task control: model-reference ISMC for compliance and robustness

As discussed before, the task coordinate of interest is the radial position r (in the cylindrical/spherical coordinate system), which can be determined by the joint coordinates q. The relevant Jacobian, $J(q)$, of the task coordinate r is defined as

$$J = \frac{\partial r}{\partial q}. \tag{2}$$

Considering kinematic redundancy of thumb and ring fingers (i.e., the dimension of the task is strictly less than the dimension of the configuration space), the following pseudo inverse as in refs. [42] and [43] is used

$$\bar{J} = M^{-1} J^T (J M^{-1} J^T)^{-1}. \tag{3}$$

Thus, using Eq. (2) allows us to project joint space dynamics (Eq. (1)) into the task space dynamics of the radius r as follows:

$$\bar{M}(q)\ddot{r} + \bar{V}(q, \dot{q})\dot{r} + \bar{G}(q) + \bar{D}_f = F, \tag{4}$$

where $\bar{M}(q) = (J M^{-1} J^T)^{-1}$, $\bar{V} = \bar{J}^T V - M\dot{J}\dot{q}$, $\bar{G} = \bar{J}^T G$ and $F = \bar{J}^T \tau$. For control, estimates of all system parameters are needed, i.e., $\hat{\bar{M}}$ is the estimate for $\bar{M}$ while $\hat{\bar{V}}$, $\hat{\bar{G}}$ are the two other respective estimates. Friction and other un-modelled forces are $\bar{D}_f = \bar{J}^T D_f$. A typical feedback linearization controller (see ref. [14], pp. 330) with PD controller is

$$F_0 = \hat{\bar{M}}(q) f^* + \hat{\bar{V}}(q, \dot{q})\dot{r} + \hat{\bar{G}}(q), \tag{5}$$

where $f^* = \ddot{r}_d(t) + K_i r_e + K_s \dot{r}_e$ and r_e is a radial error defined as $r_e(t) = r_d(t) - r(t)$ with $[r_d(t)\ \dot{r}_d(t)\ \ddot{r}_d(t)]$ being the reference trajectory and its time derivatives. Multiplying J in Eq. (5), the task space control is obtained as follows:

$$\tau_{\text{task}} = J^T (F_0 + F_1), \tag{6}$$

where F_1 is to be defined next: note that the Eq. (5) contains an estimate of the finger dynamics. These estimates are generically not easily obtained so that the estimation error

$$(\bar{M}\ddot{r}_d + \bar{V}(q, \dot{q})\dot{r} + \bar{G}(q) - \hat{\bar{M}}\ddot{r}_d - \hat{\bar{V}}(q, \dot{q})\dot{r} - \hat{\bar{G}}(q)),$$

[(1)]For control, the forces D_f do not need to be known, as sliding mode control can effectively counteract them. For active compliance, some of these forces will be measurable to be augmented into the compliance control scheme.

https://doi.org/10.1017/S0263574714002811 Published online by Cambridge University Press

and also the additional forces $\bar{D}_f$ need to be compensated for by a robust control term. Although these errors can be significant, they are in general amplitude bounded. Thus, the task controller, F_0 in Eq. (6), is now to be augmented by the ISMC, F_1; this will introduce controller robustness and also a reference model behaviour for active compliance control.

3.1.1. Integral sliding mode controller. Now, by using the ISMC approach,[38] the task control torque is extended by the nonlinear sliding mode term F_1 (Eq. (6):

$$F_1 = -\Gamma_0 \left(\frac{s}{\| s \| + \delta} \right), \quad \delta > 0, \quad \Gamma_0 > 0, \tag{7}$$

and

$$s = \dot{r}_e + K_s r_e + K_i \int_0^t r_e d\xi - \int_0^t G_f f_s d\xi - \dot{r}_e(t=0) - K_s r_e(t=0), \tag{8}$$

where $r_e(0)$ and $\dot{r}_e(0)$ are initial conditions. The gain G_f is a positive scalar and f_s is an external force measurement, obtained via specially introduced sensors.[(2)] Consider that $\int_0^t (\cdot) d\xi$ are integrals over time with integrant ξ. Moreover, it is easily seen that $s(t=0) = 0$[(3)] , which is in particular a result of the included initial values $\dot{r}_e(t=0)$ and $r_e(t=0)$. As it will be discussed in greater detail later and as it was indicated in the first paragraph of Section 3, the aim for the controller is to follow a mass-spring-damper reference model, which is obtained for $s = 0$.

Following the analysis of ref. [38], the sliding mode term enforces $s = 0$ for $\delta \to 0+$ and large enough $\Gamma_0 > 0$. The scalar $\delta > 0$ is introduced to avoid any possible chattering in the control action due to the nonlinear sliding mode term. Since $s(t=0) = 0$, it follows for large $\Gamma_0 > 0$ and for $\delta > 0$ that $\|s(t)\|$ is uniformly bounded by a bound proportional to the small value of $\delta > 0$ for all time $t \geq 0$ (see also Appendix for a stability analysis). This in general also reduces high-amplitude control action and chattering.[38] The sliding mode control term F_1 is in particular necessary, when there is model uncertainty (i.e., $\bar{M} \neq \hat{\bar{M}}$, $\bar{V}(q, \dot{q}) \neq \hat{\bar{V}}(q, \dot{q})$, $\bar{G}(q) \neq \hat{\bar{G}}(q)$), unknown uncertainty $\bar{D}_f \neq 0$ and externally sensed forces $f_s \neq 0$. We can expect that any of these terms is bounded so that a practical choice for Γ_0 is possible.

Considering that from $s = 0$ follows $\dot{s} = 0$, sliding motion $s = 0$ implies that the following second order dynamics govern for $s = \dot{s} = 0$ each robot finger

$$\ddot{r}_e + K_s \dot{r}_e + K_i r_e = G_f f_s, \quad (\text{if } s = 0), \tag{9}$$

where K_s is a damping coefficient and K_i is a stiffness coefficient of the reference model. Thus, in case sliding motion is satisfied, i.e., $s = 0$, then $\lim_{t\to\infty} r_e(t) = 0$ for a vanishing external force $f_s = 0$ only, following the dynamics of a second-order system. For $f_s \neq 0$ and $s = 0$, the external force signal influences the stable second order dynamics, replicating a mass-spring-damper system subject to an external force, i.e., in general $r_e \neq 0$; this will be discussed in greater detail in Section 4, using the idea of a virtual model with virtual coordinate r_r. In fact, it is the aim that the radial coordinate follows the virtual model coordinate r_r, i.e., $r = r_r$ for $s = 0$.

It is important to note that in contrast to former work, the introduction of the external signal, f_s, into the reference model of Eq. (9), in particular also for the operational space control context, creates a novel robust ISMC based compliance control approach.

3.1.2. Stability and robustness. The ISMC has been a well-investigated control method due to its robustness.[44–46] Following the definition of s in Eq. (8), sliding motion (i.e., $s = 0$ is reached) for the ISMC occurs right from the start of the control action, i.e., robustness is guaranteed starting from $t = 0$. Thus, by exploiting this advantage, nonlinear friction and stiction can be eliminated from the BERUL fingers. Moreover, the task motion is unaffected by posture motion. Task motion has priority

[(2)]In the case of the BERUL hand, we have used single-point tactile sensors (SPTS) which allow for force sensing at the BERUL fingertips; see Section 5 for further detail.

[(3)]Note that this is implied from $s(t=0) = \dot{r}_e(t=0) + K_s r_e(t=0) + K_i \int_0^{t=0} r_e d\xi - \int_0^{t=0} G_f f_s d\xi - \dot{r}_e(t=0) - K_s r_e(t=0) = 0$.

https://doi.org/10.1017/S0263574714002811 Published online by Cambridge University Press

over posture motion. For this, a rigorous stability analysis for this is carried out in the Appendix using the procedure of ref. [38].

It is important to note, the ISMC can be considered almost a model free design strategy where accurate information of friction/stiction, mass and Coriolis forces are not accurately required. Note that this holds as the actuator torques τ, in Eq. (1), directly affects the rigid body dynamics. This is in particular also permissible as sensors and actuators of the BERUL hand are fast and not subjected to any slow dynamics or delays. Moreover, it has been shown that the ISMC is superior in the context of trajectory following for the BERUL hand subjected to friction, in comparison to many other control methods.[39,41]

3.2. Posture control for grasping

The posture controllers are meant to regulate the remaining degrees of freedom, which are not controlled by the task controller. The index and the thumb fingers have both two actuators to control their fingertip position in terms of radial position and posture. The idea for the posture is to minimize a cost function, $U(q)$, which guarantees a certain "optimal" (nominal) positioning of the redundant degrees of freedom. In case of refs. [13] and [40], this was an effort minimizing cost function based on the effects of gravity. This has induced human like motion for a robot torso and arm control. In our case, the effects of gravity are too strongly varying with the hand movement so that a more specific hand posture cost independent of gravity is needed here.

We consider the thumb and the index finger which have two actuated degrees of freedom, q_1 and q_2. The geometric projection matrix

$$N^T = (I - J^T \bar{J}^T) = (I - J^T (J M^{-1} J^T)^{-1} J M^{-1}), \tag{10}$$

is important for the posture task, as it defines the null space of the task controller (note that the ring finger discussed here in this paper has only one actuator where all joints are connected through a pushrod. For this finger $N = 0$). It is easily seen that $\bar{J}^T N^T = 0$ and $N^T N^T = N^T$.

The overall control signal for a BERUL finger can be written as

$$\tau = J^T (F_0 + F_1) + \hat{N}^T \left(-K_{dp} \dot{q} - K_{SL} \frac{\hat{M} \hat{s}}{\| \hat{s} \| + \delta_{SL}} \right), \tag{11}$$

where $K_{dp} > 0$, $K_{SL} > 0$, $\delta > 0$ and $\hat{N}$ is computed from Eq. (10) using the mass estimate $\hat{M}$ instead of the exact value M. The variable $\hat{s}$

$$\hat{s} = B \left(\dot{q} + K_v (\frac{\partial U}{\partial q})^T \right), \tag{12}$$

introduces a sliding mode variable for the posture control where

$$B = (I - J^T (J J^T)^{-1} J). \tag{13}$$

The matrix B is a projection matrix similar to N^T, which is complemented by

$$\hat{B} = J^T (J J^T)^{-1} J. \tag{14}$$

Hence, for instance, it is easily verified that $J B = 0$ and $B + \hat{B} = I$, which subsequently also implies $\hat{B} B = 0$, $B \hat{B} = 0$, $B B = B$ and $\hat{B} \hat{B} = \hat{B}$. In the ideal case, the nonlinear sliding mode term enforces $\hat{s} = 0$ for $\delta_{SL} \to 0+$. This is achieved irrespective model uncertainties and un-modelled forces (e.g., gravity, friction and stiction), which makes the posture control robust to system uncertainty[40] in contrast to ref. [13] (see also a robustness analysis of the controller in the Appendix using ref. [40]). Thus, this robust gradient descent approach minimizing $U(q)$ is preferred for our hand control case.

3.3. Posture control with enforced gradient descent at $\hat{s} = 0$

It was mentioned before that the task control has priority over the posture, i.e., the task control is not influenced by the posture control. In contrast, the posture control is influenced by task motion. Thus,

https://doi.org/10.1017/S0263574714002811 Published online by Cambridge University Press

although $\hat{s} = 0$ can be achieved within finite time (see Appendix for analysis), the minimizing effect of the posture controller is best seen for the case $B = I$ (see also ref. [40]). This is only possible if all degrees of freedom q_1 and q_2 are part of the posture control scheme (which is in general not the case).

The general case, implies from $\hat{s} = 0$

$$B\dot{q} = -K_v B \left[\frac{\partial U}{\partial q}\right]^T. \tag{15}$$

Thus, considering that

$$\dot{U}(q) = \left[\frac{\partial U}{\partial q}\right]\dot{q} = \left[\frac{\partial U}{\partial q}\right](B + \hat{B})\dot{q}, \tag{16}$$

we obtain

$$\dot{U}(q) = -K_v \left|\left|\frac{\partial U}{\partial q} B\right|\right|^2 + \left[\frac{\partial U}{\partial q}\right]\hat{B}\dot{q}. \tag{17}$$

This shows that the sliding mode element in the posture controller introduces gradient descent via $-K_v||\frac{\partial U}{\partial q}B||^2$ to minimize $U(q)$. In particular, for $B = I$, $\dot{U}(q) = -K_v||\frac{\partial U}{\partial q}||^2$. In general, $B \neq I$ and $\hat{B} \neq 0$ which implies that the cost function is still decreasing but a trade-off has to be made due to the task control, which has priority over the posture controller. This is observed in Eq. (17), where the last term is generally non-zero for $\hat{B} \neq 0$. Hence, a cost optimization of U is limited/influenced by the task of the finger end position.

To note again, the control in Eq. (11) shows for a generic manipulator problem that $\hat{s} = 0$ is achieved for large enough gain $K_{SL} > 0$ (see Appendix and the work in ref. [40]), in particular when the robot manipulator is affected by friction and the controller lacks model knowledge. Thus, a robust posture control (Eq. (11)) is defined.

4. Compliance Control and Model Reference Behaviour

4.1. Compliance

For compliance, we reconsider the sliding variable s in Eq. (8) and its derivative

$$\dot{s} = \ddot{r}_e + K_s\dot{r}_e + K_i r_e - G_f f_s. \tag{18}$$

When sliding motion is achieved, then $s = 0$ and in particular $\dot{s} = 0$. For $\dot{s} = 0$, the error dynamics are defined by the (damping) constant K_s, the (spring) constant K_i and the external force measurement signal f_s introduced via the input distribution gain G_f, i.e., Eq. (9). This defines a reference model of Eq. (9) allowing for active compliance control via the external force signal f_s.

This contrasts to the recent use of ISMC, e.g., refs. [38] and [39] where the sliding mode dynamics generally define a nominal closed loop behaviour without external signals. This is an important tool as the controller guarantees a well-defined level of compliance despite the high degree of uncertainty and friction in the robot hands.

In practice, it is not always possible to obtain $s = 0$ in Eq. (8) at all times. Thus, it is sensible to introduce a virtual model similar to Eq. (9), as Eq. (9) only holds for $s = 0$. A virtual demand model with the coordinate r_r for this is

$$\ddot{r}_r = -K_s\dot{r}_r - K_i r_r + G_f f_s + K_s\dot{r}_d + K_i r_d + \ddot{r}_d, \tag{19}$$

using the initial conditions $r_r(t = 0) = r(t = 0)$ and $\dot{r}_r(t = 0) = \dot{r}(t = 0)$. This implies for $R_e = r_r - r_d$ that

$$\ddot{R}_e + K_s\dot{R}_e + K_i R_e = G_f f_s,$$

https://doi.org/10.1017/S0263574714002811 Published online by Cambridge University Press

which is identical to the reference model of Eq. (9) (note again that Eq. (9) is only valid once $s = 0$).

Thus, this implies from Eq. (8) and after subtraction of the integrated Eq. (19) the following:

$$\begin{aligned} s(t) &= (\dot{r}(t) - \dot{r}_r(t)) + K_s(r(t) - r_r(t)) + K_i \int_0^t (r(\xi) - r_r(\xi))d\xi \\ &\quad - (\dot{r}(0) - \dot{r}_r(0)) - K_s(r(0) - r_r(0)), \\ &= (\dot{r}(t) - \dot{r}_r(t)) + K_s(r(t) - r_r(t)) + K_i \int_0^t (r(\xi) - r_r(\xi))d\xi. \end{aligned} \tag{20}$$

Hence, for $s = 0$, $\tilde{r} = r_r - r = 0$ and in particular $\tilde{r}(t) = 0$ for all $t > 0$ when $r_r(t = 0) = r(t = 0)$, $\dot{r}_r(t = 0) = \dot{r}(t = 0)$. Thus, the joint coordinates r have to follow the virtual demand r_r in the ideal case of $s = 0$, given an original demand r_d. Hence, the relationship of Eq. (20) is an important alternative expression for s of Eq. (8) focussing on the reference model of Eq. (19) which is equivalent to Eq. (9) for $s = 0$. Thus, it is used here only for analysis, while the Eq. (8) is to be used in the implementation.

4.2. A virtual mass-spring-damper reference and computation of compliance level for an object

It is noted that for $s = 0$ follows from (9) that $r_r = r$ and

$$\frac{r_e(s)}{f_s(s)} = \frac{G_f}{s^2 + K_s s + K_i}, \tag{21}$$

where $K_s = 2\zeta\omega_n$ and $K_i = {\omega_n}^2$. The scalars ζ and ω_n are damping ratio and natural frequency respectively. Thus, different K_s, K_i and G_f to be used in order to obtain compliance levels.

The reference model cannot be arbitrarily determined and it needs to be bespoke, suitably adjusted to the context of the object handled by the robot fingers, in particular when considering the steady state force equilibrium. For this, let us consider the following mass-spring-damper system:

$$\ddot{r}_e + \frac{c_v}{m_v}\dot{r}_e + \frac{k_v}{m_v}r_e = \frac{1}{m_v}f_s, \tag{22}$$

where m_v is a virtual mass of the spring, c_v is a virtual damping constant and k_v is a virtual spring constant. By equating Eq. (22) with Eq. (9) the following relations are obtained:

$$\frac{c_v}{m_v} = 2\zeta\omega_n = K_s; \quad \frac{k_v}{m_v} = {\omega_n}^2 = K_i; \quad G_f f_s = \frac{1}{m_v}f_s, \tag{23}$$

where $G_f = \frac{1}{m_v}$. The target is now to determine c_v, k_v and m_v via suitable practical tests and design requirements for compliance and transient behaviour. We may assume that ζ and ω_n are given to establish a suitable transient behaviour, which fixes $\frac{c_v}{m_v}$ and $\frac{k_v}{m_v}$. The sensitivity to the measured force is adjusted through the input gain $G_f = \frac{1}{m_v}$.

It is now the aim to find G_f in a semi-automated process. This is to be carried out once, before any new compliant interaction task, which is to ensure safe interaction after this initial tuning process. The software-implemented process is given as follows (see also Fig. 5).

1. G_f is set to a significantly large initial value which will make the reference model highly sensitive to any external signal f_s. A task controller is initiated for a constant demand r_d. For the finger to reach r_d, it would have to penetrate the touched object, which is assumed to be stationary.
2. The finger is controlled via r_d so that it touches the object, as the demanded radius r_d is set smaller than the actual radius of the object. Any significant high pressure during the touching process is to be avoided by the compliance controller and an adjusted value r_r in Eq. (19). The initial large $G_f > 0$ makes the reference model highly sensitive to a touching interaction of the object with the finger. Once the finger has contacted the object, a sensor signal f_s is measured. Since a constant target value for r_d is set, the sensor signal f_s is steadily increasing.

https://doi.org/10.1017/S0263574714002811 Published online by Cambridge University Press

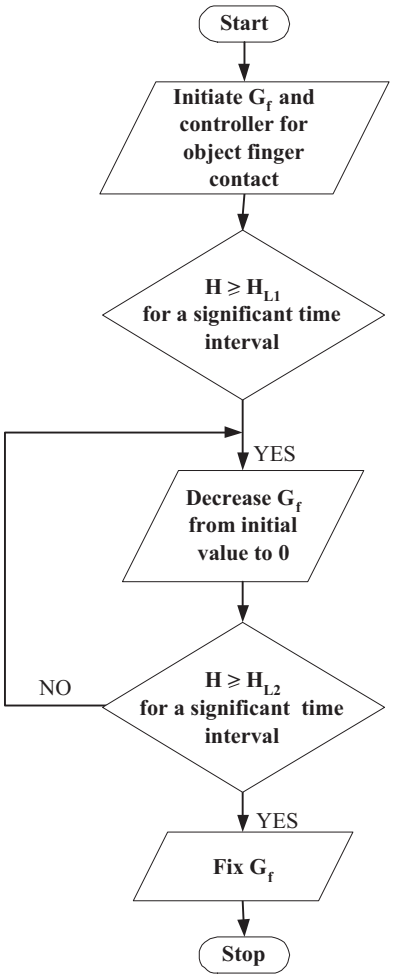

Fig. 5. Automated input distributed gain (G_f) (see itemized explanation).

3. A level F_{L1} is used to *initiate the tuning process* for G_f. Hence, once the sensor signal f_s is larger than F_{L1} for a well-defined period of time (4–5 sampling instances), the value of G_f is very slowly decreased in an automated fashion. This will make the reference model less sensitive to f_s, increase the magnitude of f_s and force r_r to be closer to r_d in Eq. (19).
4. Once the force sensor signal, f_s, has surpassed a level F_{L2}, ($F_{L2} \geq F_{L1}$) the decreasing value of G_f is kept fixed. Hence, the choice F_{L2} *defines the maximum force applied to the object and therefore determines the compliance level of the reference model* via the fixed parameters K_s, K_i and G_f. These values are now available for further use.

In summary, the process above allows to introduce a compliance reference model for a specific object-finger force interaction force level F_{L2} in a semi-automated manner. This is to be carried out once for the reference model, to be used later for the specific class of object in robot-object interaction.

5. Experimental Setup and Results

The experimental setup for the BERUL fingers is shown in Fig. 6. As a real-time interface, the dSPACE DS1006 Controller Board is used to interact with the BERUL fingers for rapid prototyping of control algorithms. Hence, the motors actuating the pushrod are driven by an EPOS brushless DC motor driver unit and the angular position of the motor is read by means of an incremental encoder. The EPOS motor drivers at each joint are in fact connected to the dSPACE system by a CAN communication bus. The control signals sent via this CAN bus, are managed by a CANopen communication protocol

https://doi.org/10.1017/S0263574714002811 Published online by Cambridge University Press

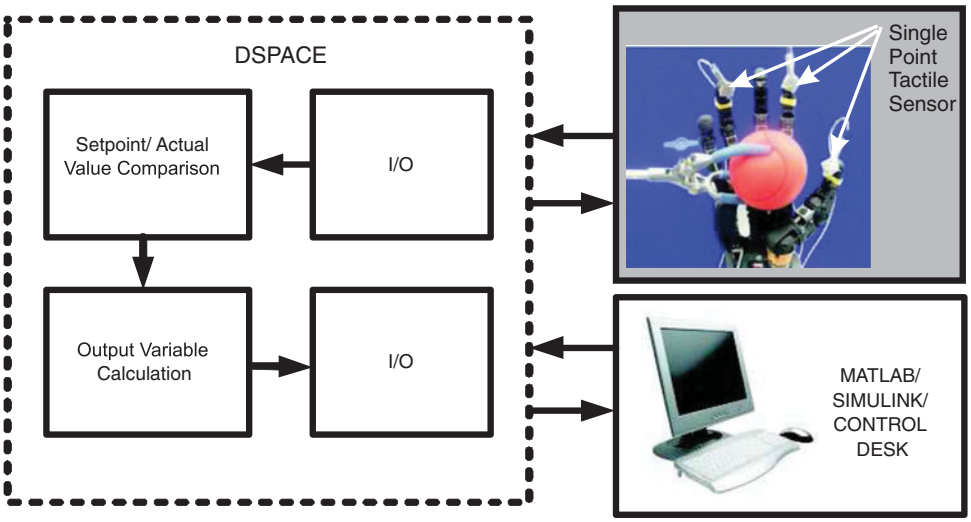

Fig. 6. Experimental setup for BERUL finger.

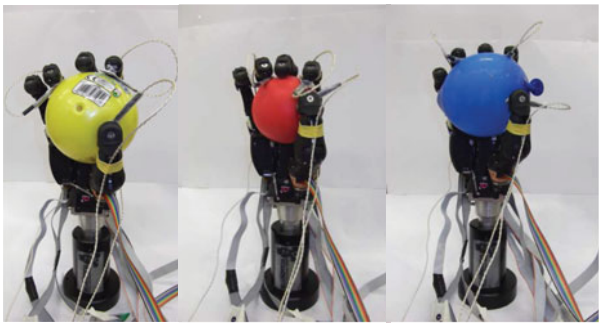

(a) Rubber Ball (b) Spongy Ball (c) Balloon

Fig. 7. Tested objects for practical compliance. (a) Rubber Ball. (b) Spongy Ball. (c) Balloon.

using a periodic synchronization signal. This allows a deterministic communication to be established in the CAN network without polling. The control loops are running at a sampling frequency of 1 kHz. Note that any computational effort needed for the nonlinear controller is negligible at this sampling frequency.

The results are divided into five different cases. Case 1 looks at the compliant behaviour of the task controller determined by a fixed reference model. Case 2 investigates the effectiveness of the posture controller, which is important for pre-grasping/object-approach hand posture and positioning. Case 3 is looking at task tracking performance of all the fingers, while posture control ensures correct finger positioning for pre-grasping and grasping. Case 4 shows the performance for different compliance levels in the task controller for a specific object. A *hard* rubber ball (Fig. 7) is used to show the results for Case 4. Case 5 demonstrates the effectiveness of the ISMC compliance controller for different objects. A *hard* spongy ball (Fig. 7(b)) and a *soft* balloon (Fig. 7(c)) are used to show the results for Case 5.

The ConTacts C500 *S*ingle-*P*oint *T*actile *S*ensors from Pressure Profile Inc.[47] (see Fig. 6) are mounted on the fingers in particular for the thumb, the index and the ring fingers; they are used to grasp various objects. Thus, only three fingers have been tested namely ring, index and thumb finger for practicality and also due to availability of three SPTSs only (it is not unusual to use three finger hands for practical grasping[6]). The SPTS has a diameter of 1 cm and it has a pressure output voltage relationship which can be approximated to about 1379 Pa = 2 psi per 1 V. Considering the area of the sensor this relates to 4.33 N per 1 V across the pad of the SPTS. The SPTS uses capacitive-based conformable pressure sensors to accurately and reliably quantify applied forces. The analogue voltage outputs are fed back into the controller for force measurement to be used for f_s in Eq. (8).

https://doi.org/10.1017/S0263574714002811 Published online by Cambridge University Press

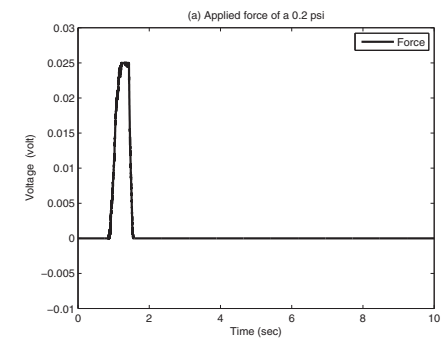

(a) Pressure sensor

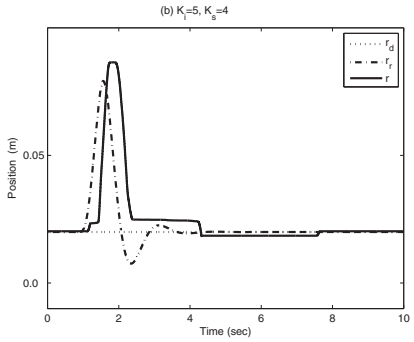

(b) Position r, r_r and r_d for $K_i = 5$, $K_s = 4$ and $G_f = 2.28, \omega = 2.23, \zeta = 0.894$

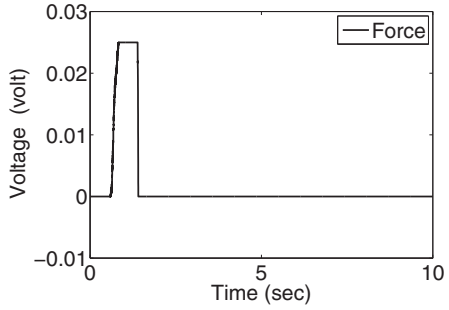

(c) Pressure sensor

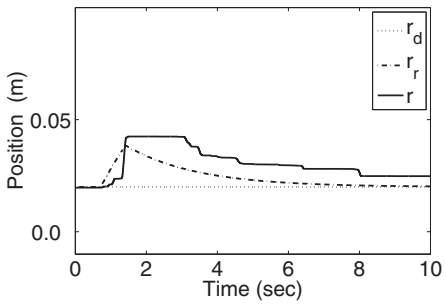

(d) Position r, r_r and r_d for $K_i = 5$, $K_s = 25$ and $G_f = 2.28, \omega = 2.23, \zeta = 5.59$

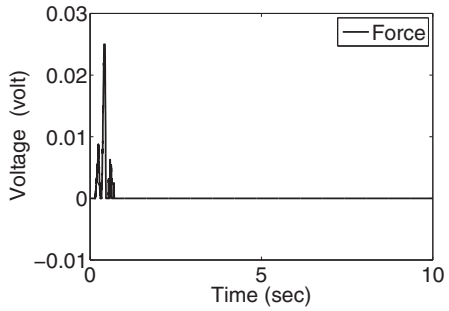

(e) Pressure sensor

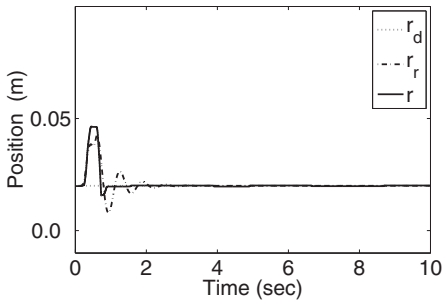

(f) Position r, r_r and r_d for $K_i = 25$, $K_s = 4$ and $G_f = 2.28, \omega = 5, \zeta = 0.4$

Fig. 8. Compliance/impedance performance for thumb and applied pressure amplitude of 0.2 psi. (a) Pressure sensor. (b) Position r, r_r and r_d for $K_i = 5$, $K_s = 4$ and $G_f = 2.28$, $\omega = 2.23$, $\zeta = 0.894$. (c) Pressure sensor. (d) Position r, r_r and r_d for $K_i = 5$, $K_s = 25$ and $G_f = 2.28$, $\omega = 2.23$, $\zeta = 5.59$. (e) Pressure sensor. (f) Position r, r_r and r_d for $K_i = 25$, $K_s = 4$ and $G_f = 2.28$, $\omega = 5$, $\zeta = 0.4$.

5.1. Compliance/impedance for different stiffness and damping – case 1

The analysis of different compliance characteristics for the ring finger are discussed in this section. It is noted that from Eq. (23) follows $K_s = 2\zeta\omega_n$ and $K_i = \omega_n^2$. Thus, different K_s and K_i are selected in order to observe compliance levels, while $G_f = 2.28$ remains fixed.

The compliance model reference behaviour is experimentally tested by exerting a calibrated force of the same amplitude to be sensed by the ISMC algorithm as shown in Figs. 8(a), (c) and (e). This is easily achieved by capping the externally sensed short burst force to the amplitude of 0.025 V (=0.108 N). For this, the actual demand r_d is kept constant. In Figs. 8(b), (d) and (f), compliance control results are provided, r_d is the original demand, r_r is the demand calculated from the virtual reference model of Eq. (19) for the actual radial position r is for the thumb finger. Thus, we use a spherical coordinate system in the case of the thumb as this will ultimately work for radial thumb abduction (in contrast to ring and index finger using cylindrical coordinates). The results clearly

https://doi.org/10.1017/S0263574714002811 Published online by Cambridge University Press

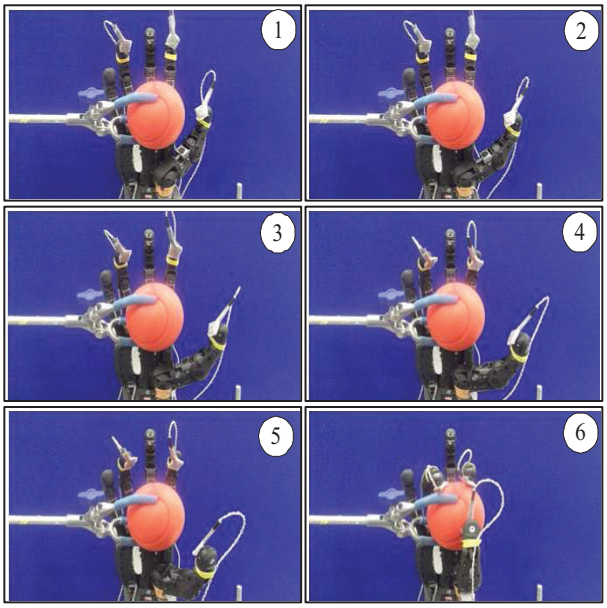

Fig. 9. Approach and grasp scenario; cylindrical coordinate space for index and ring fingers; spherical coordinate space for thumb finger (pre-grasping in subfigures 1–5; grasping in subfigure 6).

show that our design for a reference model is effective in creating active compliance. This can be seen in Fig. 8(d) where by increasing K_s (i.e., increasing the damping coefficient to $\zeta = 5.59$) the compliance controller becomes sluggish. On the other hand by increasing K_i (i.e., increasing the spring coefficient), the compliance becomes more stiff and fast, as seen in Fig. 8(f).

5.2. Posture controller parameters and results – case 2

For the experimental case 2, the robot hand is kept in upward position, while a tube holder is used to hold a ball with a diameter of about 6 cm slightly to the left of the centre point of the spherical coordinate system used for the thumb (see Fig. 9, subfigure 1). The gains used for the posture controller in particular for the index finger are $K_{dp} = 2$, $K_{SL} = 16$, $K_v = 4$, $w_1 = 3$ and $w_2 = 3$. The nominal joint positions ϕ_1 and ϕ_2 are chosen as $\phi_1 = 0.45$ rad and $\phi_2 = 1.5$ rad. This in fact defines a finger in a slightly bent, almost-open hand position. Thus, once the task controller is enabled (task control has priority over posture), the nominal "almost-open" finger posture (following ergonomics studies in ref. [10]) will guarantee that the finger encloses the object; this is visible in the motion capture of Fig. 9, subfigures 2–5. (Note that the ring finger does not require any posture control.) On the other hand, the gains for the thumb finger are $K_{dp} = 2$, $K_{SL} = 160$, $K_v = 4$, $w_1 = 2$ and $w_2 = 2$. The nominal positions of the thumb are $\phi_1 = -2.5$ rad and $\phi_2 = 1.5$ rad. They enforce for the thumb finger to move from an initial (open hand) position (see Fig. 9, subfigures 1–5) to a position where the thumb is in front of the object (Fig. 9, subfigure 6). This permits, for instance, correct positioning of the thumb before grasping, to assure a safe enclosure of an object to be grasped. Hence, although the task controller has priority to achieve the correct *radial fingertip position*, the posture controller guarantees that the redundant degrees of freedom of the hand permit practical, ergonomics-based grasping positions,[10] which is not achievable via task control only.

5.3. Tracking results – case 3

In this case, the task controller is assessed without considering any hand-object interaction to allow accurate task control tracking assessment. Thus, the hand is again kept upright, while no object is brought into the vicinity of the hand. This will imply $f_s = 0$ and $r_r = r_d$ in this case. Considering the results from case 2, the reference model parameters of Eq. (9) have been chosen as follows: $K_s = 8$ and $K_i = 18$ which implies $\omega_n = 4$ and $\zeta = 0.9$. Hence, the choice of $\omega_n = 4$ and $\zeta = 0.9$ will guarantee an approximate settling time of 1 s for a slightly underdamped reference model. The results show that, while maintaining a desired posture motion (e.g., Fig. 9), the tracking for r can be

https://doi.org/10.1017/S0263574714002811 Published online by Cambridge University Press

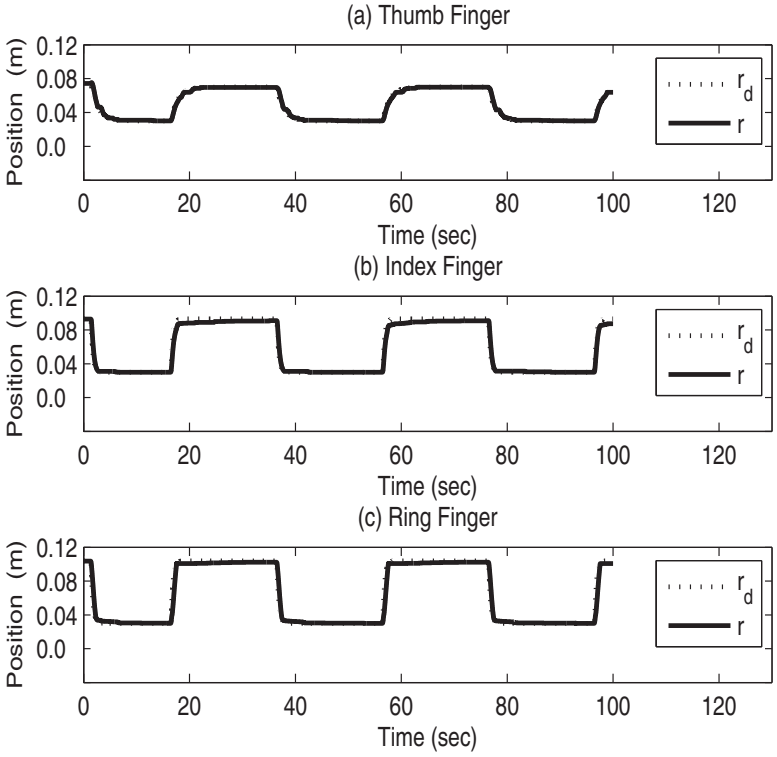

Fig. 10. (a) r_d-tracking for thumb finger in Spherical coordinates, (b) and (c) r_d-tracking for index and ring fingers in cylindrical coordinates. (a) Thumb finger. (b) Index finger. (c) Ring finger.

achieved (see Fig. 10). Moreover, the results also show that the fingers satisfactorily follow a desired trajectory (i.e., r follows r_d) during the hand opening and the hand closing period. More specifically, the task controller performance is very good despite the posture controller forces the index finger to retain an "open" finger position as much as possible. This is clearly a result of the operational space approach, i.e., the prioritization of the task controller over the posture control.

5.4. Compliance level results for an object – case 4

The automated compliance level search procedure of Section 4.2 is investigated for grasping of a *hard* rubber ball with a diameter of about 8 cm (see Fig. 7(a)). The ball is first lightly held by the tube holder, slightly left of the spherical coordinate centre, while the tube holder is then carefully removed to test the grasping process (see Fig. 9 versus Fig. 7). We have investigated two different options for the permissible contact forces F_{L2}. The level $F_{L2} = 0.01$ V(0.0433 N) and later $F_{L2} = 0.04$ V(0.1733 N). These force levels are chosen to enable object grasping without damaging the object (and also the robot hand). The lower force $F_{L2} = 0.01$ V(0.0433 N) permits a very light grasp, just avoiding object slippage.

The results reveal that a suitable reference model for both F_{L2} can be satisfactorily achieved for both levels as shown in Figs. 11 and 12 within the first 10 s. It shows that different levels of compliance are feasible for the same object. Moreover, the suggested technique to capture an appropriate G_f is reliable since it can be repeated.

Moreover, in Figs. 11 and 12, the compliance control action for fixed $G_f = const.$, $G_f > 0$, is assessed. This can be seen after a period of 60 s. Note that during the period from 40 to 60 s the fingers are open (i.e., not grasping).

It is also visible, in particular for the ring finger (Figs. 11 and 12) that the pressures exerted on the object must be higher for $F_{L2} = 0.04$ V(0.1733 N) in contrast to $F_{L2} = 0.01$V(0.0433 N), since r_d and r_r are slightly closer together. Generally, the gain G_f is larger for $F_{L2} = 0.01$ V(0.0433 N) in relation to $F_{L2} = 0.04$ V(0.1733 N) (see Tables I and II). Note the rather nonlinear relationship between F_{L2} and G_f for the two options. The decrease of G_f from $F_{L2} = 0.01$ V(0.0433 N) to

https://doi.org/10.1017/S0263574714002811 Published online by Cambridge University Press

Table I. Desired force for level 0.0433 N (0.01 V) – hard rubber ball.

Finger	G_f	F_{L2} (V)
Thumb	9.519	0.01
Index	9.959	0.01
Ring	9.993	0.01

Table II. Desired force for level 0.1733N (0.04V) – hard rubber ball.

Finger	G_f	F_{L2} (V)
Thumb	8.349	0.04
Index	9.851	0.04
Ring	9.118	0.04

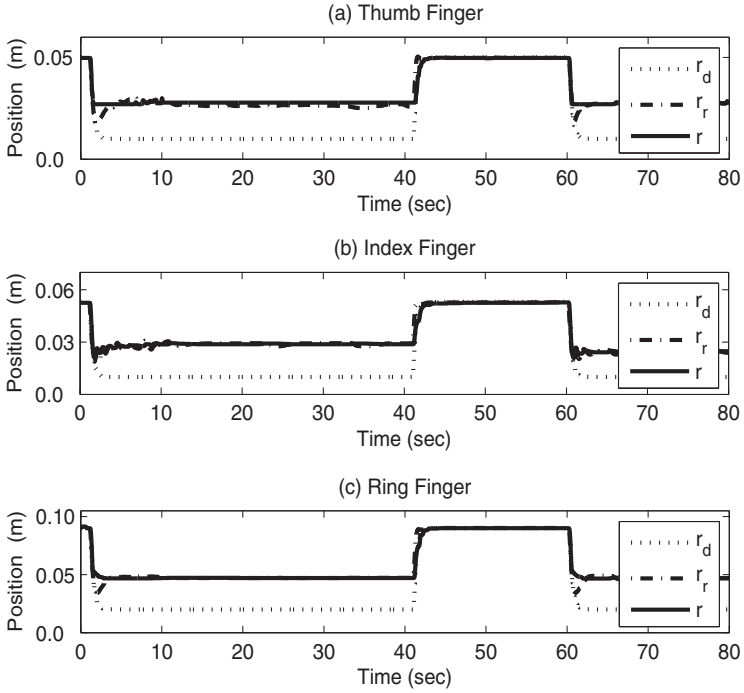

Fig. 11. Compliance performance for level 0.0433 N (0.01V). (a) Thumb Finger. (b) Index Finger. (c) Ring Finger.

$F_{L2} = 0.04$ V(0.1733 N) appears to be small, but is was found to be a repeatable result. The small difference in G_f for $F_{L2} = 0.04$V(0.1733 N) and $F_{L2} = 0.01$V(0.0433 N) may be explained by the material properties of the touched object.

5.5. Compliance level results for different objects – case 5

The automated compliance level search procedure of Section 4.2 is again used to find the compliance model investigated for a *hard* spongy ball (diameter ∼6 cm) and a *soft* balloon (diameter ∼7 cm). The results show that the automatic adjustment approach is feasible to classify compliance models for a *hard* spongy ball as shown in Table III in contrast to a *soft* balloon as shown in Table IV. The experimental process is identical to case 4, i.e., the tube holder is used to position the touched object, while it is later removed to test if the object is securely grasped.

We have chosen $F_{L2} = 0.02$ V, a force level which enables grasping of both objects. Quite clearly, a soft balloon requires a smaller G_f for the reference model, as it is easier compressed. Hence,

https://doi.org/10.1017/S0263574714002811 Published online by Cambridge University Press

Table III. Desired force for level 0.0866 N (0.02 V) – hard spongy ball.

Finger	G_f	F_{L2} (V)
Thumb	9.810	0.02
Index	9.969	0.02
Ring	9.998	0.02

Table IV. Desired force for level 0.0866 N (0.02 V) – soft balloon.

Finger	G_f	F_{L2} (V)
Thumb	9.689	0.02
Index	9.866	0.02
Ring	9.401	0.02

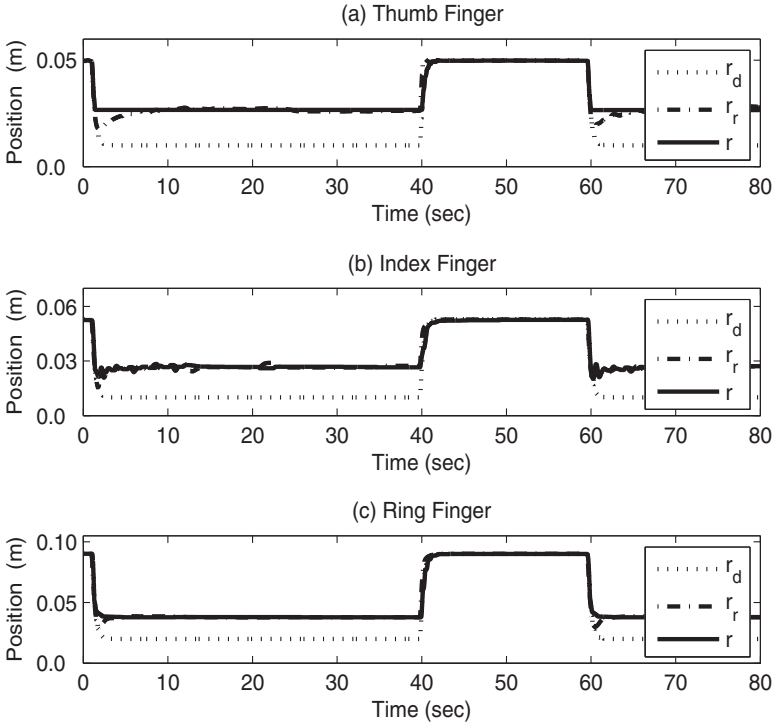

Fig. 12. Compliance performance for level 0.1733 N (0.04 V). (a) Thumb Finger. (b) Index Finger. (c) Ring Finger.

the fixed force level of $F_{L2} = 0.02$V (see Tables III and IV) implies a smaller G_f, i.e., a "stiffer" reference model.

5.6. Discussion

It is important to note that the results of this paper provide a robust, applicable approach which allows practical (power) grasping and well-measured, object-specific robust compliance. This is enabled by a synergy of techniques: operational space approach, robust ISMC in task motion for introduction of compliant control reference models and optimal posture motion to guarantee posture. As posture motion is secondary to task motion, any possible issues concerning work space are resolved indirectly: the posture control will attempt to optimize the desirable, ergonomically justified cost, while adhering to any limitations given by the hand kinematics. At the same time, compliant grasping is achieved by the ISMC-based active compliant control. The compliant controller is following a well-defined reference model, while it is fully independent from significant model parameter uncertainty of the BERUL robot hand. This for instance contrasts the work of Gioioso *et al.*,[9] where forces are dependent

https://doi.org/10.1017/S0263574714002811 Published online by Cambridge University Press

on finger and object coordinate and motion relative to each other, resulting from a detailed theoretical analysis.

6. Conclusions

In this paper, we propose a novel approach for active compliance control via ISMC. The ISMC allows us to introduce a model reference approach where a virtual mass-spring-damper system can be used to design a compliant control. The finger motion is controlled by a posture controller and a task controller as parts of an operational space controller. Both controllers use sliding mode methods to ensure robustness. Results show that the task controller can achieve indeed good tracking performance despite high levels of stiction and friction. The idea of using cylindrical and spherical coordinates and the posture controller of the index and thumb finger guarantees that both fingers move around the touched object without collision. This will allow for approach for (power) grasping and practical (power) grasping via the chosen geometry.

The tactile pressure sensors are mounted on the BERUL fingers to permit only a desired force level to affect any object. The effectiveness of the compliant control when grasping similar objects has been successfully demonstrated at different desired force levels via an automated tuning procedure. The method is also suitable for achieving compliance levels for different objects. The automated tuning process has shown that reference models for particular force levels and different objects can be easily achieved. It shows that higher desired forces require a “stiffer" reference model. For a given constant interaction force, soft objects imply also a “stiffer" reference model as these objects are easily compressed.

Acknowledgements

This project received partially funds from CHRIS (Cooperative Human Robot Interaction Systems, 2008–2012) project of the European Commission’s Seventh Framework Programme (FP7). This research was also partially funded by the Malaysian Government.

References

1. S. Jacobsen, J. Wood, D. Knutti and K. Biggers, “The utah/m.i.t. dextrous hand: Work in progress,” *Int. J. Robot. Res.* **3**(4), 21–50 (1984).
2. Shadow Robot Company, “Design of a Dextrous Hand for Advanced CLAWAR Applications,” *Proceedings of CLAWAR* (2003) pp. 691–698.
3. M. Grebenstein, A. Albu-Schaffer, T. Bahls, M. Chalon, O. Eiberger, W. Friedl, R. Gruber, S. Haddadin, U. Hagn, R. Haslinger, H. Hoppner, S. Jorg, M. Nickl, A. Nothhelfer, F. Petit, J. Reill, N. Seitz, T. Wimbock, S. Wolf, T. Wusthoff and G. Hirzinger, “The DLR Hand Arm System,” *Proceedings of the IEEE International Conference on Robotics and Automation (ICRA)* (May 2011) pp. 3175–3182.
4. C. Borst, M. Fischer, S. Haidacher, H. Liu and G. Hirzinger, “DLR Hand II: Experiments and Experience with an Anthropomorphic Hand,” *Proceedings of the IEEE International Conference on Robotics and Automation*, *ICRA ’03,* Vol. 1 (Sep. 2003) pp. 702–707.
5. W. B. Griffin, R. P. Findley, M. L. Turner and M. R. Cutkosky, “Calibration and Mapping of a Human Hand for Dexterous Telemanipulation,” *Proceedings of the ASME IMECE 2000 Symposium on Haptic Interfaces for Virtual Environments and Teleoperator Systems* (2000) pp. 1–8.
6. D. Akin, C. Carignan and A. Foster, “Development of a Four-Fingered Dexterous Robot end Effector for Space Operations,” *Proceedings of the IEEE International Conference on Robotics and Automation*, Vol. 3 (2002) pp. 2302–2308.
7. T. Geng, M. Lee and M. Hlse, “Transferring Human Grasping Synergies to a Robot,” *Mechatronics*, **21**(1), 272–284 (2011).
8. H. Wang, K. H. Low, M. Y. Wang and F. Gong, “A Mapping Method for Telemanipulation of the non-Anthropomorphic Robotic Hands with Initial Experimental Validation,” *Proceedings of the IEEE International Conference on Robotics and Automation, ICRA 2005*, IEEE (2005) pp. 4218–4223.
9. G. Gioioso, G. Salvietti, M. Malvezzi and D. Prattichizzo, “Mapping Synergies from Human to Robotic Hands with Dissimilar Kinematics: An Approach in the Object Domain,” *IEEE Trans. Robot.* **29**(4), 825–837 (2013).
10. S. C. Bae, “Investigation of Hand Posture During Reach and Grasp for Ergonomic Applications,” *Ph.D. Thesis* (Ann Arbor, Michigan: University of Michigan, 2011).
11. J. Jalani, N. Mahyuddin, G. Herrmann and C. Melhuish, “Active Robot hand Compliance using Operational Space and Integral Sliding Mode Control,” *Proceedings of the IEEE/ASME International Conference on Advanced Intelligent Mechatronics (AIM)* (2013) pp. 1749–1754.

12. J. Jalani, G. Herrmann and C. Melhuish, "Robust Active Compliance Control for Practical Grasping of a Cylindrical Object via a Multifingered Robot Hand," *Proceedings of the IEEE Conference on Robotics, Automation and Mechatronics (RAM)* (2011) pp. 316–321.
13. V. DeSapio, J. Warren, O. Khatib and S. Delp, "Simulating the task-level control of human motion: a methodology and framework for implementation." *Vis. Comput.* **21**(5) 289–302 (2005).
14. B. Siciliano, L. Sciavicco, L. Villani and G. Oriolo, *Robotics: Modelling, Planning and Control* (Springer, London, 2009).
15. R. Ham, T. Sugar, B. Vanderborght, K. Hollander and D. Lefeber, "Compliant actuator designs," *IEEE Robot. Autom. Mag.* **16**(3), 81–94 (Sep. 2009).
16. M. R. Cutkosky, *Robotic Grasping and Fine Manipulation* (Kluwer Academic Publishers, Norwell, MA, USA, 1985).
17. K. L. Johnson, *Contact Mechanics* (Cambridge University Press, Cambridge, UK, 1985).
18. K. Shimoga and A. Goldenberg, "Soft robotic fingertips," *Int. J. Robot. Res.* **15**(4), 320–334 (1996).
19. L. Biagiotti, C. Melchiorri, P. Tiezzi and G. Vassura, "Modelling and Identification of Soft Pads for Robotic Hands," *Proceedings of the IEEE/RSJ International Conference on Intelligent Robots and Systems (IROS)* (2005) pp. 2786–2791.
20. T. L. Lionel Birglen and C. Gosselin, *Underactuated Robotics Hand* (Springer-Verlag, Berlin, Heidelberg, 2008).
21. H. BenAmor, A. Saxena, N. Hudson and J. Peters, "Special issue on autonomous grasping and manipulation," *Auton. Robots* **36**(1-2), 1–3 (2014).
22. H. Liu and G. Hirzinger, "Cartesian Impedance Control for the DLR Hand," *Proceedings of the Intelligent Robots and Systems, IROS'99*, Vol. 1 (1999) pp. 106 –112.
23. C. Ott, A. Albu-Schaffer, A. Kugi and G. Hirzinger, "On the passivity-based impedance control of flexible joint robots," *IEEE Trans. Robot.* **24**(2), 416–429 (2008).
24. A. Albu-Schaffer, C. Ott and G. Hirzinger, "A unified passivity-based control framework for position, torque and impedance control of flexible joint robots," *Int. J. Robot. Res.* **26**(1), 23–39 (2007).
25. S. Khan, G. Herrmann, A. Pipe and C. Melhuish, "Safe adaptive compliance control of a humanoid robotic arm with anti-windup compensation and posture control," *Int. J. Soc. Robot.* **2**(3), 305–319 (2010).
26. Z. Chen, N. Lii, T. Wimboeck, S. Fan, M. Jin, C. Borst and H. Liu, "Experimental Study on Impedance Control for the Five-Finger Dexterous Robot Hand DLR-HIT II," *Proceedings of the IEEE/RSJ International Conference on Intelligent Robots and Systems (IROS)* (2010) pp. 5867–5874.
27. K. Mouri, K. Terashima, P. Minyong, H. Kitagawa and T. Miyoshi, "Identification and Hybrid Impedance Control of Human Skin Muscle by Multi-Fingered Robot Hand," *Proceedings of the IEEE/RSJ International Conference on Intelligent Robots and Systems, (IROS)* (2007) pp. 2895–2900.
28. Y. Xu and R. Paul, "On Position Compensation and Force Control Stability of a Robot with a Compliant Wrist," *Proceedings of the IEEE International Conference on Robotics and Automation*, Vol. 2 (Apr. 1988) pp. 1173–1178.
29. A. Jaura, M. Osman and N. Krouglicof, "Hybrid Compliance Control for Intelligent Sssembly in a Robot Work Cell," *Int. J. Prod. Res.* **36**(9), 2573–2583 (1998).
30. B.-H. Kim, S.-R. Oh, I. Suh and G.-J. Yi, "A compliance control strategy for robot manipulators under unknown environment," *KSME Int. J.* **14**, 1081–1088 (2000).
31. S. Khan, G. Herrmann, T. Pipe and C. Melhuish, "Adaptive Multi-Dimensional Compliance Control of a Humanoid Robotic Arm with Anti-Windup Compensation," *Proceedings of the IEEE/RSJ International Conference on Intelligent Robots and Systems (IROS)* (2010) pp. 2218–2223.
32. S. Haddadin, F. Huber, K. Krieger, R. Weitschat, A. Albu-Schaffer, S. Wolf, W. Friedl, M. Grebenstein, F. Petit, J. Reinecke and R. Lampariello, "Intrinsically Elastic Robots: The Key to Human like Performance," *Proceedings of the IEEE/RSJ International Conference on Intelligent Robots and Systems (IROS)* (2012) pp. 4270–4271.
33. C. Ott, B. Henze and D. Lee, "Kinesthetic Teaching of Humanoid Motion based on Whole-Body Compliance Control with Interaction-Aware Balancing," *Proceedings of the IEEE/RSJ International Conference on Intelligent Robots and Systems (IROS)* (2013) pp. 4615–4621.
34. H. Sadeghian, M. Keshmiri, L. Villani and B. Siciliano, "Null-Space Impedance Control with Disturbance Observer," *Proceedings of the IEEE/RSJ International Conference on Intelligent Robots and Systems (IROS)* (2012) pp. 2795–2800.
35. T. Zhang, L. Jiang, S. Fan, X. Wu and W. Feng, "Development and experimental evaluation of multi-fingered robot hand with adaptive impedance control for unknown environment grasping," *Robotica* (FirstView) **10,** 1–18 (2014).
36. T. Zhang, L. Jiang, X. Wu, W. Feng, D. Zhou and H. Liu, "Fingertip three-axis tactile sensor for multifingered grasping," *IEEE/ASME Trans. Mechatronics* **PP**(99), 1–11 (2014).
37. T. Zhang, H. Liu, L. Jiang, S. Fan and J. Yang, "Development of a flexible 3-d tactile sensor system for anthropomorphic artificial hand," *IEEE Sensors J.*, **13**(2), 510–518 (2013).
38. J. Shi, H. Liu and N. Bajcinca, "Robust control of robotic manipulators based on integral sliding mode," *Int. J. Control* **81**, 1537–1548 (2008).
39. J. Jalani, G. Herrmann and C. Melhuish, "Underactuated fingers controlled by robust and adaptive trajectory following methods," *Int. J. Syst. Sci.* **45**(2), 120–132 (2014), DOI: 10.1080/00207721.2012.687866.

40. A. Spiers, G. Herrmann and C. Melhuish, "An Optimal Sliding Mode Controller Applied to Human Motion Synthesis with Robotic Implementation," *American Control Conference (ACC)* (Jun. 30–Jul. 2 2010) pp. 991–996.
41. J. Jalani, G. Herrmann and C. Melhuish, "Robust Trajectory Following for Underactuated Robot Fingers," *Proceedings of the UKACC International Conference on CONTROL* (Sep. 2010) pp. 495–500.
42. O. Khatib, "A unified approach for motion and force control of robot manipulators: The operational space formulation," *IEEE J. Robot. Autom.* **3**(1), 43–53 (1987).
43. O. Khatib, "Inertial properties in robotic manipulation: An object-level framework," *Int. J. Robot. Res.*, **14**(1), 19–36 (1995).
44. M. Yokoyama, G.-N. Kim and M. Tsuchiya, "Integral sliding mode control with anti-windup compensation and its application to a power assist system," *J. Vib. Control* **16**(4), 503–512 (2010).
45. M. Defoort, T. Floquet, A. Kokosy and W. Perruquetti, "Integral sliding mode control for trajectory tracking of a unicycle type mobile robot," *Integr. Comput.-Aided Eng.* **13**(3), 277–288 (2006).
46. I. Eker and S. Akinal, "Sliding mode control with integral augmented sliding surface: Design and experimental application to an electromechanical system," *Electr. Eng.*, **90**(3), 189–197 (2008).
47. Pressure Profile Systems, Inc. ConTacts C500 Single-Point Tactile Sensor (2014). http://www.pressureprofile.com.fqdns.net/UserFiles/File/PPS%20_ConTacts_Specsheets_08_18_10.pdf?PHPSESSID=8a2d3964082f7b93e2f3cfd0f8598cfd.

Appendix. Stability analysis

The appendix summarizes in a brief manner a stability argument for the control scheme, considering ideas of refs. [38] and [40].

Appendix.1. Task motion

Fact 1. The task motion is not influenced by the posture controller if the mass estimate $\hat{M} = M$ is correct.

This is known from operational space control.[13,42,43]

Proof. This fact is easily obtained from the following line of argumentation:

The combined controller of task and posture controller is given by Eq. (11), while the task motion trajectory r is described by the dynamics of Eq. (4). Note that the dynamics of Eq. (4) are the result of a nonlinear transformation. In particular, the virtual input force/torque F is defined by $F = \bar{J}^T \tau$, where $\bar{J}$ is defined in Eq. (3). Note that $\bar{J}^T N^T = 0$. Moreover, $\hat{N} = N$ for $\hat{M} = M$. Thus, using the definition $F = \bar{J}^T \tau$, it follows from Eq. (11)

$$\begin{aligned} F &= \bar{J}^T \tau \\ &= \bar{J}^T \left(J^T (F_0 + F_1) + N^T (-K_{dp} \dot{q} - K_{SL} \frac{\hat{\bar{M}} \hat{s}}{\| \hat{s} \| + \delta_{SL}}) \right) \\ &= F_0 + F_1. \end{aligned} \tag{24}$$

□

Thus, task motion is not influenced by the posture controller. The next step is to show robust stability of the task control, in particular that the sliding mode variable s in Eq. (8) remains 0 for $\delta = 0$:

Lemma 1. *Provided that* Γ_0 *is large enough, the sliding mode variable s remains within a small compact set containing the origin* 0*. For* $\delta = 0$*, s remains 0 at all times.*

The proof of this lemma is based on the ideas of ref. [38].

Proof. At first, consider the sliding variable s (8) and its derivative $\dot{s}$:

$$\dot{s} = \ddot{r}_e + K_s \dot{r}_e + K_i r_e - G_f f_s. \tag{25}$$

https://doi.org/10.1017/S0263574714002811 Published online by Cambridge University Press

The control law $F = F_0 + F_1 + \bar{J}^T(\hat{N} - N)^T(-K_{dp}\dot{q} - K_{SL}\frac{\hat{\bar{M}}\hat{s}}{\|\hat{s}\|+\delta_{SL}})$ from Eqs. (5) and (7) implies for the task control dynamics of Eq. (4).

$$\begin{aligned}\bar{M}\ddot{r}_e + \bar{M}K_s\dot{r}_e + \bar{M}K_i r_e - \bar{M}G_f f_s = {} & (\hat{\bar{M}} - \bar{M})f^* + (\hat{\bar{V}}(q,\dot{q})\dot{r} - \bar{V}(q,\dot{q})\dot{r}) \\ & + (\hat{\bar{G}}(q) - \bar{G}(q)) - \bar{D}_f - \bar{M}G_f f_s \\ & + \bar{J}^T(\hat{N} - N)^T\left(-K_{dp}\dot{q} - K_{SL}\frac{\hat{\bar{M}}\hat{s}}{\| \hat{s} \| + \delta_{SL}}\right) \\ & - \Gamma_0\left(\frac{s}{\| s \| + \delta}\right),\end{aligned}$$

or equivalently

$$\begin{aligned}\bar{M}\dot{s} = {} & (\hat{\bar{M}} - \bar{M})f^* + (\hat{\bar{V}}(q,\dot{q})\dot{r} - \bar{V}(q,\dot{q})\dot{r}) \\ & + (\hat{\bar{G}}(q) - \bar{G}(q)) - \bar{D}_f - \bar{M}G_f f_s \\ & + \bar{J}^T(\hat{N} - N)^T\left(-K_{dp}\dot{q} - K_{SL}\frac{\hat{\bar{M}}\hat{s}}{\| \hat{s} \| + \delta_{SL}}\right) - \Gamma_0\left(\frac{s}{\| s \| + \delta}\right).\end{aligned}$$

Consider the following function $V_s = \frac{1}{2}s^T s$. Computing the temporal derivative, it follows:

$$\begin{aligned}\dot{V}_s = {} & s^T\dot{s} \\ = {} & s^T\bar{M}^{-1}\left((\hat{\bar{M}} - \bar{M})f^* + (\hat{\bar{V}}(q,\dot{q})\dot{r} - \bar{V}(q,\dot{q})\dot{r})\right) \\ & + s^T\bar{M}^{-1}(\hat{\bar{G}}(q) - \bar{G}(q)) - s^T\bar{M}^{-1}\bar{D}_f - s^T G_f f_s \\ & + s^T\bar{M}^{-1}\bar{J}^T(\hat{N} - N)^T\left(-K_{dp}\dot{q} - K_{SL}\frac{\hat{\bar{M}}\hat{s}}{\| \hat{s} \| + \delta_{SL}}\right) - s^T\bar{M}^{-1}\Gamma_0\left(\frac{s}{\| s \| + \delta}\right).\end{aligned}$$

This implies

$$\begin{aligned}\dot{V}_s \leq {} & s^T\bar{M}^{-1}\left((\hat{\bar{M}} - \bar{M})f^* + (\hat{\bar{V}}(q,\dot{q})\dot{r} - \bar{V}(q,\dot{q})\dot{r})\right) \\ & + s^T\bar{M}^{-1}(\hat{\bar{G}}(q) - \bar{G}(q)) - s^T\bar{M}^{-1}\bar{D}_f - s^T G_f f_s \\ & + s^T\bar{M}^{-1}\bar{J}^T(\hat{N} - N)^T\left(-K_{dp}\dot{q} - K_{SL}\frac{\hat{\bar{M}}\hat{s}}{\| \hat{s} \| + \delta_{SL}}\right) - \Gamma_0\frac{\lambda_{\min}(\bar{M}^{-1})\,\|s\|^2}{\| s \| + \delta} \\ = {} & s^T\bar{M}^{-1}\left((\hat{\bar{M}} - \bar{M})f^* + (\hat{\bar{V}}(q,\dot{q})\dot{r} - \bar{V}(q,\dot{q})\dot{r})\right) \\ & + s^T\bar{M}^{-1}(\hat{\bar{G}}(q) - \bar{G}(q)) - s^T\bar{M}^{-1}\bar{D}_f - s^T G_f f_s \\ & + s^T\bar{M}^{-1}\bar{J}^T(\hat{N} - N)^T\left(-K_{dp}\dot{q} - K_{SL}\frac{\hat{\bar{M}}\hat{s}}{\| \hat{s} \| + \delta_{SL}}\right) - \Gamma_0\lambda_{\min}(\bar{M}^{-1})\,\|s\| \\ & + \Gamma_0\frac{\lambda_{\min}(\bar{M}^{-1})\,\|s\|\,\delta}{\| s \| + \delta},\end{aligned}$$

https://doi.org/10.1017/S0263574714002811 Published online by Cambridge University Press

and

$$\begin{aligned}\dot{V}_s \leq & \left\| \bar{M}^{-1}\left((\hat{\bar{M}}-\bar{M})f^* + (\hat{\bar{V}}(q,\dot{q})\dot{r} - \bar{V}(q,\dot{q})\dot{r})\right)\right. \\ & \left. + \bar{M}^{-1}(\hat{\bar{G}}(q) - \bar{G}(q)) - \bar{M}^{-1}\bar{D}_f - G_f f_s - \bar{M}^{-1}\bar{J}^T(\hat{N}-N)^T K_{dp}\dot{q}\right\| \|s\| \\ & + \left\|\bar{M}^{-1}\bar{J}(\hat{N}-N)^T\right\| K_{SL}\|\hat{\bar{M}}\|\,\|s\| - \Gamma_0\lambda_{\min}(\bar{M}^{-1})\,\|s\| + \Gamma_0\lambda_{\min}(\bar{M}^{-1})\delta \\ \leq & \left(\left\| \bar{M}^{-1}\left((\hat{\bar{M}}-\bar{M})f^* + (\hat{\bar{V}}(q,\dot{q})\dot{r} - \bar{V}(q,\dot{q})\dot{r})\right)\right.\right. \\ & \left. + \bar{M}^{-1}(\hat{\bar{G}}(q) - \bar{G}(q)) - \bar{M}^{-1}\bar{D}_f - G_f f_s - \bar{M}^{-1}\bar{J}^T(\hat{N}-N)^T K_{dp}\dot{q}\right\| \\ & \left. + \left\|\bar{M}^{-1}\bar{J}(\hat{N}-N)^T\right\| K_{SL}\|\hat{\bar{M}}\|\right)\sqrt{2}\sqrt{V_s} \\ & - \Gamma_0\lambda_{\min}(\bar{M}^{-1})\sqrt{2}\sqrt{V_s} + \Gamma_0\lambda_{\min}(\bar{M}^{-1})\delta.\end{aligned}$$

Assuming

$$\begin{aligned}\Gamma_0\lambda_{\min}(\bar{M}^{-1}) > & \left\|\bar{M}^{-1}\Big((\bar{M}-\hat{\bar{M}})f^* + (\bar{V}(q,\dot{q}) - \hat{\bar{V}}(q,\dot{q}))\dot{r} + \bar{G}(q) - \hat{\bar{G}}(q) + \bar{D}_f\Big) - G_f f_s\right. \\ & \left. - \bar{M}^{-1}\bar{J}^T(\hat{N}-N)^T K_{dp}\dot{q}\right\| + \left\|\bar{M}^{-1}\bar{J}(\hat{N}-N)^T\right\| K_{SL}\|\hat{\bar{M}}\|, \qquad (26)\end{aligned}$$

and the assumption of $s(t=0)=0$, it is evident that the sliding variable s remains within a compact set for which the radius is proportional to δ. For $\delta = 0$, it follows that $s(t) = 0$ for all time $t > 0$. □

The requirement of Eq. (26) provides excellent evidence why the integral sliding mode technique is almost model free; for instance, it is easily possible to assume for instance that the estimate for the Coriolis/centrifugal effects has been insufficiently modelled, i.e., $\hat{\bar{V}}(\cdot,\cdot) = 0$. This would create a higher demand on Γ_0 in Eq. (26).

It is to note, once $s(t) = 0$ is achieved, the task controller follows the ideal reference model of Eq. (9), representing an arbitrarily tunable mass-spring-damper system subject to an external force f_s. Thus, Section 4 provides a practical discussion of this reference model, which is in particular suited to evaluate how well the reference model is practically followed in the actual implementation.

Appendix.2. Posture motion

It has been emphasized that task motion takes priority over posture motion. Despite that, the posture controller is robust to model uncertainty, i.e., $\hat{s} = 0$ is achieved in case, $\delta_{SL} \to 0+$, which is summarized below using ideas from [40]:

Lemma 2. *If the matrix $M^{-1}\hat{M} + \hat{M}M^{-1}$ is strictly positive definite at all times, the variable, $\hat{s}$, is ultimately bounded, i.e., it will remain in a compact set, also containing $\hat{s} = 0$, after finite time. For $\delta_{SL} = 0$, $\hat{s} = 0$ is achieved within finite time.*

The constraint for positive definiteness of $M^{-1}\hat{M} + \hat{M}M^{-1}$ is in principle an assumption that the mass estimate, $\hat{M}$, is fairly good, which can be assumed to be correct, considering the simplicity of the robot finger dynamics. In the ideal case, $M^{-1}\hat{M} + \hat{M}M^{-1} = 2I$. The proof of the lemma is based on ref. [40].

https://doi.org/10.1017/S0263574714002811 Published online by Cambridge University Press

Proof. Consider $V_{\hat{s}} = \frac{1}{2}\hat{s}^T\hat{s}$, which implies from Eq. (1)

$$\begin{aligned}
\dot{V}_{\hat{s}} &= \hat{s}^T\dot{\hat{s}} \\
&= \hat{s}^T B\left(\ddot{q} + K_v\left(\frac{\partial^2 U}{\partial q^2}\ddot{q}\right)^T\right) + \hat{s}^T\dot{B}\left(\dot{q} + K_v\left(\frac{\partial U}{\partial q}\right)^T\right) \\
&= \hat{s}^T B\left(-M^{-1}V(q,\dot{q})\dot{q} - M^{-1}G(q) - M^{-1}D_f + M^{-1}\tau + K_v\left(\frac{\partial^2 U}{\partial q^2}\ddot{q}\right)^T\right) \\
&\quad + \hat{s}^T\dot{B}\left(\dot{q} + K_v\left(\frac{\partial U}{\partial q}\right)^T\right).
\end{aligned}$$

From $BB = B$ and (12) follows, $B\hat{s} = \hat{s}$. Moreover, defining $R = -M^{-1}V(q,\dot{q})\dot{q} - M^{-1}G(q) - M^{-1}D_f + K_v(\frac{\partial^2 U}{\partial q^2}\ddot{q})^T + \dot{B}(\dot{q} + K_v(\frac{\partial U}{\partial q})^T)$, it easily seen that

$$\dot{V}_{\hat{s}} = \hat{s}^T B(M^{-1}\tau + R). \tag{27}$$

Now, it is possible to exploit the relationships $\hat{N}^T\hat{M}B = \hat{M}B$, $B\hat{s} = \hat{s}$ and $N^T B = N^T$, so that

$$\begin{aligned}
\dot{V}_{\hat{s}} &= -K_{dp}\hat{s}^T BM^{-1}\hat{N}^T B\hat{s} - K_{SL}\hat{s}^T BM^{-1}\hat{M}B\frac{\hat{s}}{\|\hat{s}\| + \delta_{SL}} \\
&\quad + \hat{s}^T\left(-K_{dp}K_v M^{-1}\hat{N}^T\left(\frac{\partial U}{\partial q}\right)^T + BJ^T F + BR\right).
\end{aligned} \tag{28}$$

Note that $BJ^T = 0$ and using the (positive) smallest eigenvalue $\lambda_{\min}(\cdot)$ of $(M^{-1}\hat{M} + \hat{M}M^{-1})$:

$$\begin{aligned}
\dot{V}_{\hat{s}} &= -\hat{s}^T BM^{-1}N^T B\hat{s} - K_{SL}\frac{1}{2}\hat{s}^T B(M^{-1}\hat{M} + \hat{M}M^{-1})B\frac{\hat{s}}{\|\hat{s}\| + \delta_{SL}} \\
&\quad + \hat{s}^T\left(M^{-1}(N^T - \hat{N}^T)\hat{s} - K_{dp}K_v M^{-1}\hat{N}^T\left(\frac{\partial U}{\partial q}\right)^T + BR\right) \\
&\leq -K_{SL}\lambda_{\min}(M^{-1}\hat{M} + \hat{M}M^{-1})\frac{1}{2}\hat{s}^T\frac{\hat{s}}{\|\hat{s}\| + \delta_{SL}} \\
&\quad + \|\hat{s}\|\left\|\left(M^{-1}(N^T - \hat{N}^T)\hat{s} - K_{dp}K_v M^{-1}\hat{N}^T\left(\frac{\partial U}{\partial q}\right)^T + BR\right)\right\| \\
&\leq -K_{SL}\lambda_{\min}(M^{-1}\hat{M} + \hat{M}M^{-1})\frac{1}{\sqrt{2}}\sqrt{V_{\hat{s}}} \\
&\quad + \sqrt{2}\sqrt{V_{\hat{s}}}\|M^{-1}(N^T - \hat{N}^T)\hat{s} - K_{dp}K_v M^{-1}\hat{N}^T\left(\frac{\partial U}{\partial q}\right)^T + BR\| \\
&\quad + K_{SL}\delta_{SL}\frac{1}{2}\lambda_{\min}(M^{-1}\hat{M} + \hat{M}M^{-1}),
\end{aligned}$$

where the matrix $BM^{-1}N^T B$ is symmetric and positive semi-definite. Hence, for

$$K_{SL}\lambda_{\min}(M^{-1}\hat{M} + \hat{M}M^{-1})\frac{1}{2} > \|M^{-1}(N^T - \hat{N}^T)\hat{s} - K_{dp}K_v M^{-1}\hat{N}^T\left(\frac{\partial U}{\partial q}\right)^T + BR\|, \tag{29}$$

it is seen that $\hat{s}$ is entering a set of ultimate boundedness, where the radius is proportional to δ_{SL}. Hence, for $\delta_{SL} = 0$, it is possible to achieve $\hat{s} = 0$ within finite time. □

https://doi.org/10.1017/S0263574714002811 Published online by Cambridge University Press